



# Low-Complexity One-Bit DOA Estimation for Massive ULA with a Single Snapshot

Shaodi Ge , Chongyi Fan , Jian Wang and Xiaotao Huang \*

College of Electronic Science, National University of Defense Technology, Changsha 410073, China; shaodi@nudt.edu.cn (S.G.); chongyifan@nudt.edu.cn (C.F.); jianwang\_uwb@nudt.edu.cn (J.W.)

\* Correspondence: xthuang@nudt.edu.cn

**Abstract:** Existing one-bit direction of arrival (DOA) estimate methods based on sparse recovery or subspace have issues when used for massive uniform linear arrays (MULAs), such as high computing cost, estimation accuracy depending on grid size, or high snapshot-number requirements. This paper considers the low-complexity one-bit DOA estimation problems for MULA with a single snapshot. Theoretical study and simulation results demonstrate that discrete Fourier transform (DFT) can be applied to MULA for reliable initial DOA estimation even when the received data are quantized by one-bit methods. A precise estimate is then obtained by searching within a tiny area. The resulting method is called one-bit DFT. This method is straightforward and simple to implement. High-precision DOA estimates of MULA can be obtained with a single snapshot, and the computational complexity is significantly less than that of existing one-bit DOA estimation methods. Moreover, the suggested method is easily extensible to multiple snapshot scenarios, and increasing the number of snapshots can further improve estimation precision. Simulation results show the effectiveness of the one-bit DFT method.

**Keywords:** one-bit quantization; DOA estimation; single snapshot; massive ULA



**Citation:** Ge, S.; Fan, C.; Wang, J.; Huang, X. Low-Complexity One-Bit DOA Estimation for Massive ULA with a Single Snapshot. *Remote Sens.* **2022**, *14*, 3436. <https://doi.org/10.3390/rs14143436>

Academic Editors: Konrad Jędrzejewski and Matthias Weiß

Received: 6 June 2022  
Accepted: 15 July 2022  
Published: 17 July 2022

**Publisher's Note:** MDPI stays neutral with regard to jurisdictional claims in published maps and institutional affiliations.



**Copyright:** © 2022 by the authors. Licensee MDPI, Basel, Switzerland. This article is an open access article distributed under the terms and conditions of the Creative Commons Attribution (CC BY) license (<https://creativecommons.org/licenses/by/4.0/>).

## 1. Introduction

The direction of arrival (DOA) estimate is widely utilized in radar array systems, smart antenna, adaptive beamforming, and other applications as a key technology of passive radar [1–9]. In recent years, with the rapid development of massive multiple-input multiple-output (MIMO) technology, the DOA estimation method for massive antenna array has become a focus of research [10–18]. However, massive antenna array confronts several challenges, including a large number of antenna components, high computational complexity, and high power consumption, among others. Given that high-resolution quantization is preferable in signal recovery performance, its impracticality is probable due to high hardware costs and system power consumption. The analog-to-digital converter (ADC) is one of the most power-consuming devices, and its power consumption increases exponentially with quantized digits [19]. The limited hardware cost will bring severe challenges to parameter estimation and real-time signal processing. Therefore, system design using low-resolution ADCs and related signal-processing techniques has attracted great research interest [20–24].

Recently, massive MIMO systems have extensively investigated one-bit ADCs consisting of simple comparators that can significantly simplify other RF components and consume even negligible circuit power [25–30]. After one-bit quantization, only the measured symbol information is available, but it has been demonstrated that robust DOA estimates can still be ensured [31–35]. Stockle et al. [31] formulated one-bit DOA estimation as a sparse recovery problem, which was solved by extending the binary iterative hard-thresholding technique to complex-valued signals. Simulation results show that the performance of this method for one-bit DOA estimation is comparable to the subspace-based methods with multiple signal classification (MUSIC) and estimating signal parameter

via rotational invariance techniques (ESPRITs). Meng et al. [32] presented the one-bit DOA estimate with a single snapshot as a generalized linear model inference problem and solved it using the recently developed generalized sparse Bayesian learning (Gr-SBL) technique. Huang et al. [33] showed that the one-bit covariance matrix is approximable by the sum of a scaled unquantized covariance matrix and a scaled identity matrix. Based on this, a one-bit MUSIC method was developed, which directly finds the signal subspace and the noise subspace via the eigendecomposition of the one-bit covariance matrix and applies the most classical MUSIC technique to determine the DOA of the signal. Wei et al. [34] established a sparse reconstruction model for one-bit quantization based on atomic norm (one-bit AN) minimization to accomplish gridless DOA estimation. The sign inconsistency between the one-bit measurement and the actual signal is restricted by employing a linear loss function. Then, the interior point method or semidefinite programming solver was utilized to resolve it. The above one-bit methods based on sparse recovery or subspace can produce good estimation results when used to massive uniform linear arrays (MULA). Nonetheless, they have limitations such as high computational cost, estimate accuracy that is sensitive to grid size, and the need for a large number of snapshots.

Different from existing methods, we present a low-complexity one-bit DOA estimation method based on discrete Fourier transform (DFT) in this paper. DFT has been widely used in single-snapshot DOA estimation of MULA in recent years [16,36,37]. Theoretical study and simulation confirmation demonstrates that even after one-bit quantization of the single snapshot data received by MULA, the initial DOA estimation can be obtained from the DFT spectrum's peak location. Then, we search a small area for the optimal phase rotation to obtain a precise estimate. Additionally, we extend the one-bit DFT method for single-snapshot scenarios to handle multiple snapshots. The proposed method is straightforward to apply, and the high-precision estimation result of MULA can be produced from a single snapshot. The estimation performance is enhanced by increasing the number of snapshots. Simulation results indicate that the estimation precision of the proposed method is superior to that of the existing one-bit DOA estimation methods and that it also has the benefit of high computational efficiency.

The remainder of the paper is structured as follows: Section 2 reviews the one-bit signal model; Section 3 presents the proposed one-DFT method; Section 4 provides the numerical simulations and discusses the results; Section 5 concludes the paper.

## 2. One-Bit Signal Model

Consider a MULA with  $M \gg 1$  antennas that are separated by a half-wavelength. Assume there are  $K$  far-field sources impacting the array from  $\theta = [\theta_1, \dots, \theta_K]$ . Received data for a single snapshot can be represented as follows:

$$\mathbf{x} = \mathbf{A}\mathbf{s} + \mathbf{n} \quad (1)$$

where  $\mathbf{A} = [\mathbf{a}(\theta_1), \dots, \mathbf{a}(\theta_K)] \in \mathbb{C}^{M \times K}$  represents the steering matrix, and  $\mathbf{a}(\theta_k)$  is the steering vector.  $\mathbf{s} = [s_1, \dots, s_K]^T$  denotes the  $K \times 1$  complex-valued signals with different signals independent of each other obeying a circularly symmetric complex Gaussian distribution with power  $\sigma_k^2, k = 1, 2, \dots, K$ .  $\mathbf{n} \in \mathbb{C}^{M \times 1}$  represents additive white Gaussian noise with the power of  $\sigma_n^2$ . In the  $\theta_k$  direction, the steering vector is given by the following.

$$\mathbf{a}(\theta_k) = [e^{j\pi \sin \theta_k}, e^{j2\pi \sin \theta_k}, \dots, e^{jM\pi \sin \theta_k}]^T \quad (2)$$

The one-bit quantized data model can be described as follows:

$$\mathbf{y} = \frac{1}{\sqrt{2}}(\text{sign}(\text{Re}(\mathbf{x})) + j\text{sign}(\text{Im}(\mathbf{x}))) \quad (3)$$

where  $\text{sign}(\cdot)$  is an element-by-element function, which is defined as follows.

$$\text{sign}(w) = \begin{cases} 1, & \text{if } w \geq 0 \\ -1, & \text{if } w < 0 \end{cases} \quad (4)$$

### 3. Proposed Method

#### 3.1. DFT

DFT is one of the conventional non-parametric approaches for spectrum analysis. Define the normalized  $M \times M$  DFT matrix  $\mathbf{F}$ , where  $[\mathbf{F}]_{pq} = e^{-j(2\pi/M)pq} / \sqrt{M}$ . The DFT spectrum of  $\mathbf{a}(\theta_k)$  is  $\mathbf{Fa}(\theta_k)$ , and the  $q$ -th element is as follows.

$$[\mathbf{Fa}(\theta_k)]_q = \frac{1}{\sqrt{M}} \frac{\sin[\frac{M}{2}(\frac{2\pi}{M}q - \pi \sin \theta_k)]}{\sin[\frac{1}{2}(\frac{2\pi}{M}q - \pi \sin \theta_k)]} e^{-j\frac{M}{2}[\frac{2\pi}{M}q - \pi \sin \theta_k]} \quad (5)$$

If the array has an infinite number of antennas (i.e.,  $M \rightarrow \infty$ ), there is always an integer  $q_k = \frac{M}{2} \sin \theta_k$  such that  $[\mathbf{Fa}(\theta_k)]_{q_k} = \sqrt{M}$ , while all other elements of  $\mathbf{Fa}(\theta_k)$  are zero [15,38]. Thus,  $|\mathbf{Fa}(\theta_k)|$  and  $|\mathbf{Fx}|$  are ideally sparse, and the initial estimate of  $\theta_k$  can be obtained immediately from the peak position of  $|\mathbf{Fx}|$ .

$$\theta_k^{ini} = \arcsin(2q_k/M), \quad k = 1, 2, \dots, K \quad (6)$$

#### 3.2. Covariance Matrix Analysis after One-Bit Quantization

Next, we analyze the effect of one-bit quantization on the sample covariance matrix. Due to the independence between signals and between signals and noise, the mean of  $x_q = [\mathbf{x}]_q$  is zero, and the variance  $\sigma_{x_q}^2 = \mathbf{E}[x_q x_q^*]$  (i.e., the  $q$ -th diagonal term of  $\mathbf{R}_x$ ) is given by the following.

$$\sigma_{x_q}^2 = [\mathbf{R}_x]_{qq} = \sum_{k=1}^K |a_q(\theta_k)|^2 \sigma_k^2 + \sigma_n^2 \quad (7)$$

The correlation coefficient  $\rho_{x_p x_q}$  between the unquantized measurements of the  $p$ -th and  $q$ -th sensors (where  $p \neq q$ ) can be written as follows [33].

$$\begin{aligned} \rho_{x_p x_q} &= \frac{\mathbf{E}[x_p x_q^*]}{\sigma_{x_p} \sigma_{x_q}} = \frac{[\mathbf{R}_x]_{pq}}{\sqrt{[\mathbf{R}_x]_{pp}} \sqrt{[\mathbf{R}_x]_{qq}}} \\ &= \frac{\sum_{k=1}^K a_p(\theta_k) a_q^*(\theta_k) \sigma_k^2}{\sqrt{\sum_{k=1}^K |a_p(\theta_k)|^2 \sigma_k^2 + \sigma_n^2} \sqrt{\sum_{k=1}^K |a_q(\theta_k)|^2 \sigma_k^2 + \sigma_n^2}} \end{aligned} \quad (8)$$

Since  $a_p(\theta_k) = e^{jp\pi \sin \theta_k}$ , Equation (7) can be simplified as  $L = [\mathbf{R}_x]_{qq} = \sum_{k=1}^K \sigma_k^2 + \sigma_n^2$ ,  $q = 1, 2, \dots, M$ . Moreover, assuming for convenience that the signals are of equal power, i.e.,  $\delta = \sigma_k^2 / \sigma_n^2$ ,  $k = 1, 2, \dots, K$ , then there is the following:

$$\rho_{x_p x_q} = \frac{\sum_{k=1}^K e^{j(p-q)\pi \sin \theta_k}}{K + \delta^{-1}} \quad (9)$$

and  $|\rho_{x_p x_q}| < 1$ .

Consider a one-bit quantitative measurement  $y_q$ ,  $q = 1, 2, \dots, M$  with zero mean and unit variance, i.e.,  $\mathbf{E}[y_q] = 0$  and  $\sigma_{y_q}^2 = 1$ . Therefore, the correlation coefficient between  $y_p$  and  $y_q$  is as follows.

$$\rho_{y_p y_q} = \frac{1}{\sigma_{y_p} \sigma_{y_q}} \mathbf{E}[y_p y_q^*] = [\mathbf{R}_y]_{pq} \quad (10)$$

In particular, if  $p = q$ , there is  $\rho_{y_p y_p} = 1$ . According to the arcsine law [39,40], we have the following.

$$\begin{aligned}\rho_{y_p y_q} &= \frac{2}{\pi} \arcsine(\rho_{x_p x_q}) \\ &= \frac{2}{\pi} (\arcsin(\operatorname{Re}(\rho_{x_p x_q})) + j \arcsin(\operatorname{Im}(\rho_{x_p x_q})))\end{aligned}\quad (11)$$

Therefore, combining Equation (8), we can obtain the following.

$$\mathbf{R}_y = \frac{2}{\pi} \arcsine\left(\frac{1}{L} \mathbf{R}_x\right) \quad (12)$$

Equation (12) shows that the unquantized covariance matrix can be reconstructed from the one-bit covariance matrix as  $\mathbf{R}_x = L \operatorname{sine}\left(\frac{\pi}{2} \mathbf{R}_y\right)$ , where  $\operatorname{sine}(z) = \sin(\operatorname{Re}(z)) + j \sin(\operatorname{Im}(z))$ , and  $L$  is an unknown scaling parameter. The literature [33] analysis demonstrates that  $\mathbf{R}_x$  can be approximated by the sum of the scaled  $\mathbf{R}_y$  and the scaled identity matrix  $\mathbf{I}$ . First,  $\arcsin(\operatorname{Re}(\rho_{x_p x_q}))$  can be expanded as follows.

$$\arcsin(\operatorname{Re}(\rho_{x_p x_q})) = \operatorname{Re}(\rho_{x_p x_q}) + \frac{1}{6} \operatorname{Re}^3(\rho_{x_p x_q}) + \frac{3}{40} \operatorname{Re}^5(\rho_{x_p x_q}) + \dots \quad (13)$$

If  $|\operatorname{Re}(\rho_{x_p x_q})|$  is small enough (that is, SNR is low enough),  $\arcsin(\operatorname{Re}(\rho_{x_p x_q}))$  can be well approximated as  $\operatorname{Re}(\rho_{x_p x_q})$ .

$$\arcsin(\operatorname{Re}(\rho_{x_p x_q})) \approx \operatorname{Re}(\rho_{x_p x_q}) \quad (14)$$

This approximation can also be applied to  $\operatorname{Im}(\rho_{x_p x_q})$ , resulting in  $\rho_{y_p y_q} \approx \frac{2}{\pi} \rho_{x_p x_q}$ . According to Equations (12) and (14), the following is the case.

$$[\mathbf{R}_y]_{pq} \approx \frac{2}{L\pi} [\mathbf{R}_x]_{pq}, p \neq q \quad (15)$$

Since  $\rho_{y_q y_q} = \rho_{x_q x_q} = 1$ , the error caused by approximating  $\arcsin(1)$  to 1 is larger, and Equation (15) can be rewritten as [33] follows:

$$\mathbf{R}_y - \mathcal{D}(\mathbf{R}_y) \approx \frac{2}{L\pi} (\mathbf{R}_x - \mathcal{D}(\mathbf{R}_x)) \quad (16)$$

where  $\mathcal{D}(\mathbf{R}) = \operatorname{diag}(\mathbf{R}_{11}, \dots, \mathbf{R}_{MM})$  is a diagonal matrix. Due to  $[\mathbf{R}_y]_{qq} = 1$  and  $[\mathbf{R}_x]_{qq} = L$ , one can yield [33] the following.

$$\mathbf{R}_y \approx \frac{2}{L\pi} \mathbf{R}_x + \left(1 - \frac{2}{\pi}\right) \mathbf{I} \quad (17)$$

### 3.3. One-Bit DFT

For the received single snapshot data  $\mathbf{x}$  and the one-bit quantized data  $\mathbf{y}$ , there are  $\mathbf{R}_x = \mathbf{x}\mathbf{x}^H$  and  $\mathbf{R}_y = \mathbf{y}\mathbf{y}^H$ . Multiplying both sides of Equation (17) by  $\mathbf{F}$  simultaneously provides the following:

$$\begin{aligned}\mathbf{F}\mathbf{R}_y\mathbf{F}^H &\approx \mathbf{F}\left(\frac{2}{L\pi} \mathbf{R}_x + \left(1 - \frac{2}{\pi}\right) \mathbf{I}\right)\mathbf{F}^H \\ &\approx \frac{2}{L\pi} \mathbf{F}\mathbf{R}_x\mathbf{F}^H + \left(1 - \frac{2}{\pi}\right) \mathbf{I}\end{aligned}\quad (18)$$

when  $M \rightarrow \infty$ ,  $|\mathbf{F}\mathbf{x}|$  is ideally sparse, and has distinct peaks at positions  $q_k, k = 1, 2, \dots, K$  corresponding to the incident angle information. Thus, we have the following.

$$\begin{aligned} \text{diag}(\mathbf{F}\mathbf{R}_x\mathbf{F}^H) &= \text{diag}(\mathbf{F}\mathbf{x}(\mathbf{F}\mathbf{x})^H) \\ &= [\sigma_n^2, \dots, M\sigma_k^2 + \sigma_n^2, \dots, \sigma_n^2]^T \end{aligned} \tag{19}$$

In other words,  $\text{diag}(|\mathbf{F}\mathbf{R}_x\mathbf{F}^H|)$  has obvious peaks at the diagonal terms  $|\mathbf{F}\mathbf{R}_x\mathbf{F}^H|_{q_k q_k} = M\sigma_k^2, k = 1, 2, \dots, K$ . A similar conclusion is reached for the diagonal elements of  $|\mathbf{F}\mathbf{R}_y\mathbf{F}^H|$  according to Equations (18) and (19).

In fact, from Equation (17),  $\mathbf{R}_y$  has almost the same eigenvector as  $\frac{2}{L\pi}\mathbf{R}_x + (1 - \frac{2}{\pi})\mathbf{I}$ . Therefore, for the single-snapshot received data of the MULA, we do not need to multiply each side of the one-bit covariance matrix  $\mathbf{R}_y$  by  $\mathbf{F}$ . Instead, directly based on the DFT spectrum  $|\mathbf{F}\mathbf{y}|$  of  $\mathbf{y}$ , determine the corresponding angle by locating the positions of the  $K$  largest peaks  $q_k, k = 1, \dots, K$ . From Equation (5), these positions satisfy

$$\frac{1}{2} \left( \frac{2\pi}{M} q_k - \pi \sin \theta_k \right) = 0 \tag{20}$$

or

$$\frac{1}{2} \left( \frac{2\pi}{M} q_k - \pi \sin \theta_k \right) = \pi \tag{21}$$

The initial DOAs estimate can be obtained.

$$\begin{cases} \theta_k^{ini} = \arcsin(2q_k/M) & \text{if } 0 \leq q_k \leq \frac{M}{2} \\ \theta_k^{ini} = \arcsin(2(q_k - M)/M) & \text{if } \frac{M}{2} < q_k \leq M \end{cases} \tag{22}$$

Figures 1 and 2 depicts  $|\mathbf{F}\mathbf{R}_y\mathbf{F}^H|_{qq}$  and  $|\mathbf{F}\mathbf{y}|_q, q = 1, 2, \dots, M$  for a single incidence source with  $\theta = -40^\circ$  striking a 500-element MULA. At  $q_k = 339$ , there is a very significant peak that can be observed. From Equation (22), the initial estimate can be calculated as  $\theta^{ini} = -40.0907^\circ$ .

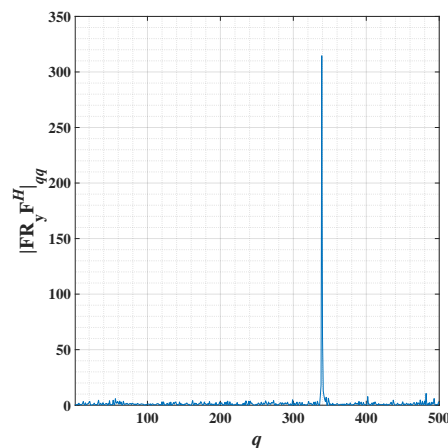
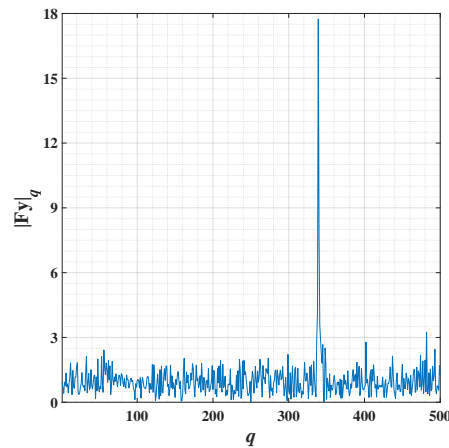


Figure 1.  $|\mathbf{F}\mathbf{R}_y\mathbf{F}^H|_{qq}, q = 1, 2, \dots, M, \text{SNR} = 0 \text{ dB}$ .



**Figure 2.**  $|\mathbf{F}\mathbf{y}|_q, q = 1, 2, \dots, M$ , SNR = 0 dB.

### 3.4. Precise Estimation

In conjunction with the preceding analysis, we can utilize the phase rotation operation to obtain a precise estimate of DOAs after the received data have been quantized by one-bit. The phase rotation is defined as  $\Phi(\eta)$ , where  $\Phi(\eta)$  is the diagonal matrix defined by  $\Phi(\eta) = \text{diag}\{e^{j\eta}, \dots, e^{jM\eta}\}$  and  $\eta \in [-\pi/M, \pi/M]$  is the corresponding phase shift [15]. Assume that the phase deviation of the initially estimated DFT spectrum is  $\eta_k$ . Referring to Equations (5), (20), and (21),  $\eta_k$  satisfies the following.

$$\frac{1}{2} \left( \frac{2\pi}{M} q_k - \eta_k - \pi \sin \theta_k^{ini} \right) = 0 \quad (23)$$

or

$$\frac{1}{2} \left( \frac{2\pi}{M} q_k - \eta_k - \pi \sin \theta_k^{ini} \right) = \pi \quad (24)$$

to maximize the peak value at  $|\mathbf{F}\Phi(\eta_k)\mathbf{y}|_{q_k}$ . Therefore, the precise estimate of  $\hat{\theta}_k$  can be calculated as

$$\hat{\theta}_k = \begin{cases} \arcsin(2\pi q_k / \pi M - \eta_k / \pi) & \text{if } \theta_k^{ini} \geq 0 \\ \arcsin(2(q_k - M) / M - \eta_k / \pi) & \text{if } \theta_k^{ini} < 0 \end{cases} \quad (25)$$

To identify the optimal offset phase,  $[-\pi/M, \pi/M]$  is divided into  $j$  grids for searching  $\eta$ . Extracting the corresponding  $\eta_k$  by searching only at the  $K$  peaks such that  $|\mathbf{F}\Phi(\eta_k)\mathbf{y}|$  is the maximum reduces the computational effort of the grid search.

$$\eta_k = \arg \max_{\eta \in (-\pi/M, \pi/M)} \|\mathbf{F}_{(q_k, :)} \Phi(\eta) \mathbf{y}\|^2, k = 1, 2, \dots, K \quad (26)$$

In Algorithm 1, we summarize the one-bit DFT method.

---

#### Algorithm 1 One-bit DFT.

---

Input: One-bit quantized data vector  $\mathbf{y}$ , number of signals  $K$ , and number of grids  $J$ .

Output:  $\hat{\theta}_k, k = 1, 2, \dots, K$ .

(1) Construct DFT matrix  $[\mathbf{F}]_{pq} = e^{-j(2\pi/M)pq} / \sqrt{M}$ ;

(2) Find the  $K$  largest peaks of  $|\mathbf{F}\mathbf{y}|$ , and obtain the initial DOA estimate according to Equation (22);

(3) Construct the phase rotation set, and obtain the optimal offset phase from Equation (26);

(4) Use Equation (25), precise estimates of  $\hat{\theta}_k, k = 1, 2, \dots, K$  can be obtained.

---

### 3.5. Expand to Multiple Snapshot Scenarios

Although this study addresses the problem of one-bit DOA estimate using a single snapshot for MULA, it is easily extensible to the case of multiple snapshots. Consider multiple snapshots with measurements of one-bit quantization:

$$\mathbf{y}_t = \frac{1}{\sqrt{2}}(\text{sign}(\text{Re}(\mathbf{x}_t)) + j\text{sign}(\text{Im}(\mathbf{x}_t))), t = 1, 2, \dots, T. \quad (27)$$

where  $T$  is the number of snapshots. According to Equations (18) and (19), the diagonal elements of  $|\mathbf{F}\mathbf{R}_x\mathbf{F}^H|$  and  $|\mathbf{F}\mathbf{R}_y\mathbf{F}^H|$  should exhibit prominent peaks at the point corresponding to the incidence angle information, where  $\mathbf{R}_x = \frac{1}{T} \sum_{t=1}^T \mathbf{x}_t\mathbf{x}_t^H$  and  $\mathbf{R}_y = \frac{1}{T} \sum_{t=1}^T \mathbf{y}_t\mathbf{y}_t^H$ . Let  $\tilde{\mathbf{y}}_t = \mathbf{F}\mathbf{y}_t$ ,  $|\mathbf{F}\mathbf{R}_y\mathbf{F}^H|_{qq}$  can be simplified as follows.

$$|\mathbf{F}\mathbf{R}_y\mathbf{F}^H|_{qq} = \frac{1}{T} \sum_{t=1}^T [\tilde{\mathbf{y}}_t]_q [\tilde{\mathbf{y}}_t]_q^H, q = 1, 2, \dots, M. \quad (28)$$

Thus, we obtain the initial angle estimate based on the peak position  $q_k, k = 1, 2, \dots, K$  of  $\text{diag}(\mathbf{F}\mathbf{R}_y\mathbf{F}^H)$ .

Next, the optimal phase rotation can be calculated as follows.

$$\eta_k = \arg \max_{\eta \in (-\pi/M, \pi/M)} \left[ \frac{1}{T} \sum_{t=1}^T \sum_{q=1}^M [\hat{\mathbf{y}}_t]_q [\hat{\mathbf{y}}_t]_q^H \right], k = 1, 2, \dots, K \quad (29)$$

where  $\hat{\mathbf{y}}_t = \mathbf{F}_{(q_k, :)} \Phi(\eta) \mathbf{y}_t$ . Finally, the precise estimation result is obtained using Equation (25).

### 3.6. Performance Analysis

The proposed method obtains initial estimate  $\theta_k^{ini}$  from the peak position of the DFT spectrum of the received data such that the worst error of  $\sin \theta_k^{ini}$  does not exceed  $2/M$  according to Equations (20) and (21) as long as the right peak locations are determined. The phase rotation procedure can enhance the precision of the initial estimation. According to Equation (25), the worst error of  $\sin \hat{\theta}_k$  does not exceed  $2/JM$ . For example, when  $J = 10$ , the worst error of  $\sin \hat{\theta}_k$  is on the order of  $10^{-3}$  for MULA with hundreds of array elements.

Compared to subspace methods such as one-bit MUSIC [33] and one-bit ESPRIT [35], the suggested method exploits the fact that large-scale antenna arrays can significantly increase the resolution of DFT-based spectral analysis, and only a single snapshot is required to obtain a more precise DOA estimate. In contrast, the one-bit MUSIC and one-bit ESPRIT methods need an eigenvalue decomposition of the sample covariance matrix, and the signal subspace cannot be built effectively when the number of signals exceeds the number of snapshots. Therefore, these two methods are incapable of accurately estimating DOA for a single snapshot.

### 3.7. Computational Complexity Analysis

The computational complexity of the one-bit DFT method mainly includes the calculation of the DFT spectrum of the received data and the phase rotation operation, and the remaining operations are relatively ignored. To calculate the DFT spectrum, FFT can be used to accelerate the calculation in actual implementation, and the complexity is in the order of  $O(TM \log M)$  [15]. The phase rotation procedure for precise estimation requires  $O(KMJT)$ , which is typically enough to generate extremely precise estimations for tiny values of  $J$ . Thus, the complexity is approximately  $O(T(M \log M + KMJ))$ . Since the received data are quantized to one-bit and contains only symbol information, it can reduce hardware costs and increase computation efficiency in practical applications.

#### 4. Simulation and Results Analysis

This section considers four equal-power narrowband signals impinging on the array from  $-40.61^\circ$ ,  $-10.37^\circ$ ,  $30.61^\circ$ , and  $60.24^\circ$ . SNR is defined as  $\text{SNR} = 10 \log_{10} \frac{E\|\mathbf{As}\|_2^2}{E\|\mathbf{n}\|_2^2} = 10 \log_{10} \frac{E\|\mathbf{As}\|_2^2}{M\sigma_n^2}$ , and compute  $\sigma_n^2$  according to the SNR [32]. Unless otherwise specified, SNR is set to 0 dB, and the number of snapshots is set to 1 in simulations.

In the first simulation, we verified the ability of the one-bit DFT method to accurately locate the sources when applied to MULA. Figure 3 shows the DFT spectrum  $|\mathbf{Fy}|$  of  $\mathbf{y}$  in a single simulation with varying array elements, and Table 1 displays the initial estimate  $\theta_k^{ini}$  based on the peak location. Prominent peaks can be seen in the DFT spectrum at position  $q_k, k = 1, 2, \dots, 4$ . As the number of array elements increases, the peak becomes more apparent, and the resulting initial estimate becomes more accurate. Figure 4 illustrates the location of the highest four peaks of the DFT spectrum of 1000 Monte Carlo tests under various array elements. The one-bit quantitative data  $\mathbf{y}$  of each Monte Carlo test were regenerated. It has been observed that the one-bit DFT method can determine the correct peak location every time and can locate sources reliably.

**Table 1.** Peak location and initial DOA estimation.

	$-40.61^\circ$		$-10.37^\circ$		$30.61^\circ$		$60.24^\circ$	
	$\theta_1^{ini}$	$q_1$	$\theta_2^{ini}$	$q_2$	$\theta_3^{ini}$	$q_3$	$\theta_4^{ini}$	$q_4$
$M = 500$	$-40.6926^\circ$	337	$-10.3698^\circ$	455	$30.5307^\circ$	127	$60.2271^\circ$	217
$M = 1000$	$-40.5416^\circ$	675	$-10.3698^\circ$	910	$30.6638^\circ$	255	$60.2271^\circ$	434
$M = 5000$	$-40.6019^\circ$	3373	$-10.3698^\circ$	4550	$30.6106^\circ$	1273	$60.2271^\circ$	2170
$M = 10,000$	$-40.6170^\circ$	6745	$-10.3698^\circ$	9100	$30.6106^\circ$	2546	$60.2501^\circ$	4341

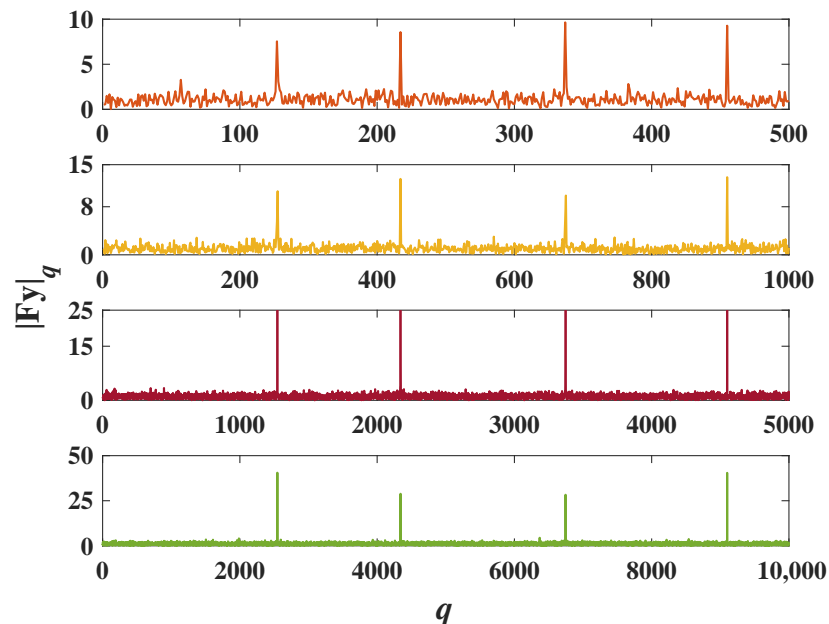


**Figure 3.** The DFT spectrum  $|\mathbf{Fy}|$  of  $\mathbf{y}$ .

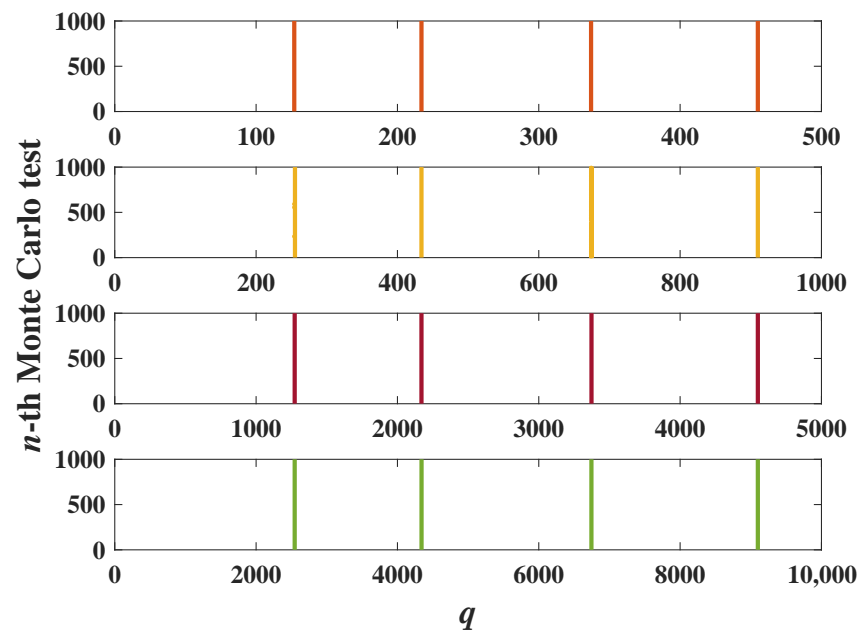


**Figure 4.** The location of the most highest four peaks obtained by the one-bit DFT method for 1000 Monte Carlo trials.

In the second simulation, the one-bit DFT method is compared with the state-of-the-art one-bit DOA estimate methods Gr-SBL [32], one-bit MUSIC [33], and one-bit AN [34]. The number of grid searches for the one-bit DFT method is  $J = 20$ . Gr-SBL and the one-bit MUSIC grid interval have been set to 0.25, meaning 721 grids in total. One-Bit MUSIC does not work efficiently with a single snapshot, so the number of snapshots is set to 10. Let us utilize the mean absolute error (MAE) to evaluate the effectiveness of all methods [41,42]:

$$\text{MAE} = \frac{1}{KN} \left( \sum_{n=1}^N \sum_{k=1}^K |\theta_k - \hat{\theta}_{k,n}| \right) \quad (30)$$

where  $N$  is the number of Monte Carlo runs and  $\hat{\theta}_{k,n}$  represents the estimated value of the incident angle  $\theta_k$  of the  $n$ -th Monte Carlo test.  $M = 500$  and  $N = 200$  are set in this simulation.

Figure 5 shows the MPE curve of all methods varying with SNR. When the input SNR is low, it is observed that estimation errors for all methods are large. Due to the limited resolution of the DFT operation, the accuracy of the initial estimate does not improve when the SNR is greater than  $-4$  dB. Even if the approximation error of Equation (17) is relatively large in the case of high SNR, the proposed method causes no performance loss in the initial estimation as long as the accurate position of the peak point is determined. After phase rotation, the accuracy of the precise estimate of one-bit DFT improves significantly and outperforms all other comparison methods. Gr-SBL and one-bit MUSIC almost always find the nearest grid point to the true DOAs when the input SNR is high, and the estimation accuracy is mainly affected by the off-grid error. However, finer meshing will significantly increase runtime. The estimation accuracy of one-bit AN is better than the initial estimation accuracy of the one-bit DFT, Gr-SBL, and one-bit MUSIC at high SNR and lower than the precise estimation of the one-bit DFT method. Figure 6 shows the average running time of all methods. The One-bit DFT method only takes about 0.1s, which is much lower than other methods.

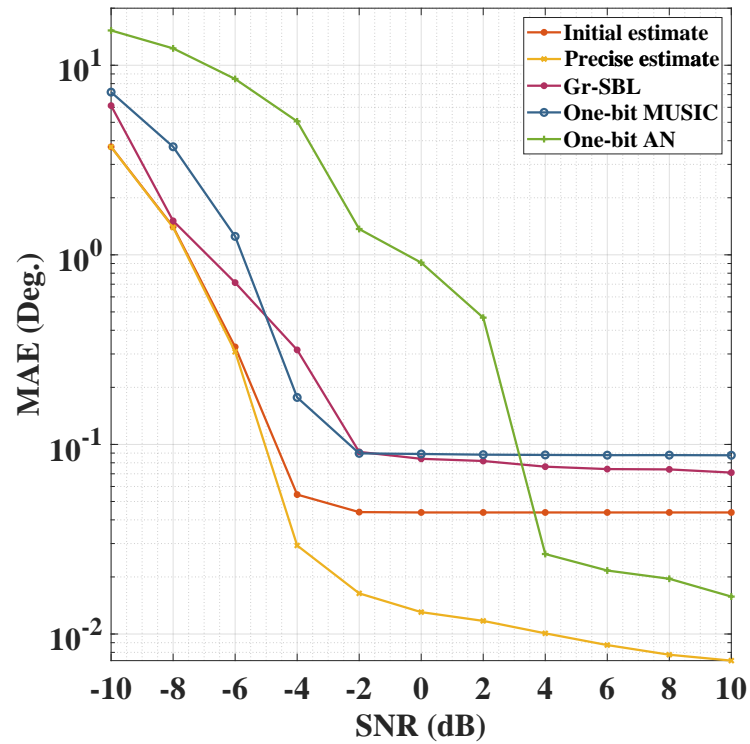


Figure 5. MAE versus SNR.

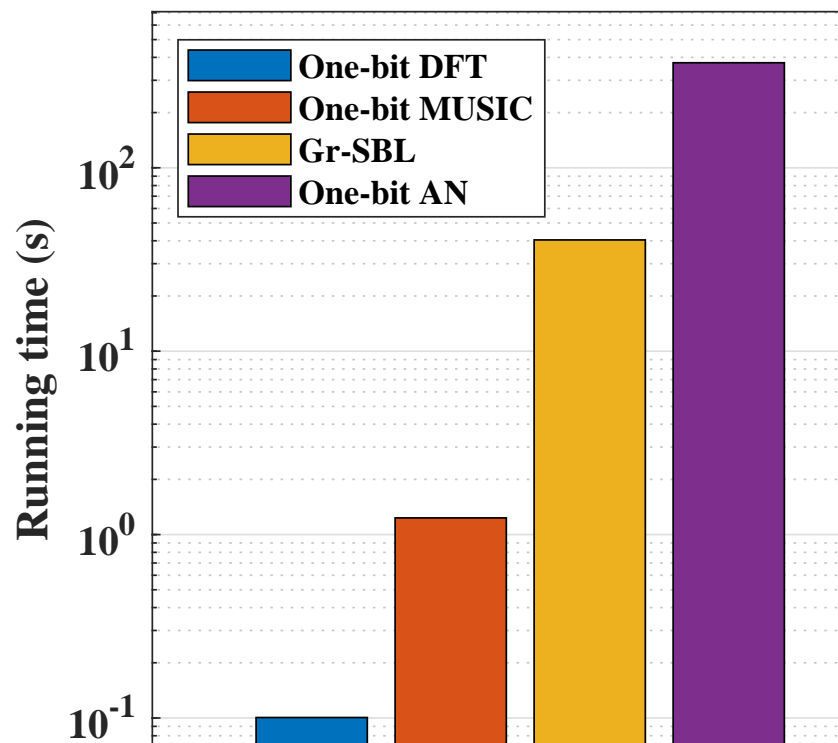


Figure 6. Average runtime comparison of all methods.

In the third simulation, the effect of snapshot number on the performance of the proposed method is evaluated. Figure 7 depicts the MAE versus SNR curve of the proposed method for varying numbers of snapshots, where  $M = 500$  and  $N = 200$ . It can be observed that, as the number of snapshots increases, the accuracy of the proposed method’s precise estimation improves.

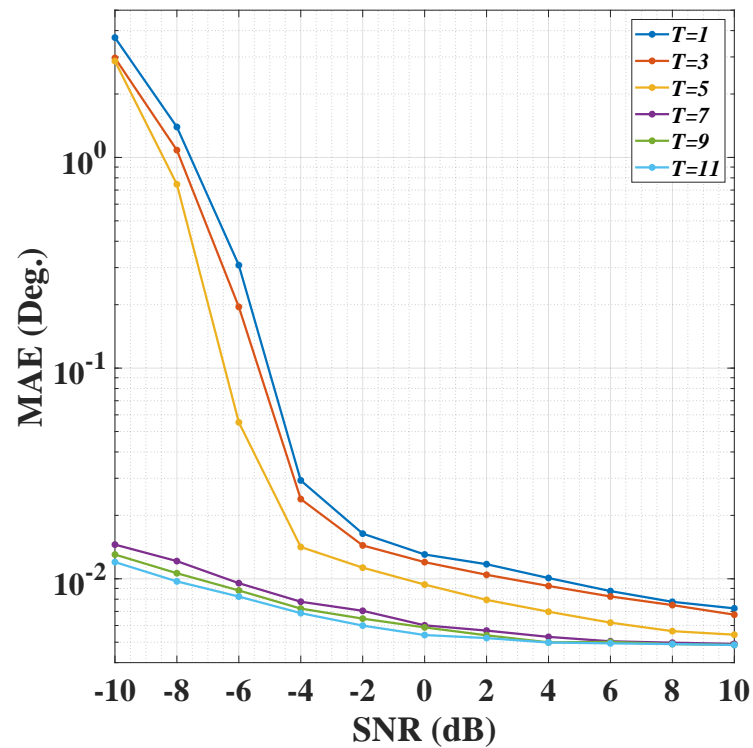


Figure 7. MAE versus SNR curve of the proposed method with different number of snapshots.

In the fourth simulation, the performance of each method is compared when incident signals have varying magnitudes. In particular, we analyze the two incident signals  $\theta_1 = -40.61^\circ$  and  $\theta_2 = 30.61^\circ$ , for which the signal magnitude in the  $\theta_1$  direction is fixed at 0 dB while the signal magnitude in the  $\theta_2$  direction varies from 0 dB to 20 dB. When the DOA estimated by all methods satisfy  $|\hat{\theta}_k - \theta_k| < 1^\circ, k = 1, 2$ , the two sources are considered to be distinguished successfully; otherwise, the resolution fails. The number of snapshots for the Gr-SBL and One-bit AN methods is set to 1, and the number of snapshots for the one-bit MUSIC method is set to 10. Additionally, we simulate the performance of the suggested method using a single snapshot and ten snapshots.

Figure 8 displays the resolution results of all methods, where the resolution probability is the ratio of the number of successful resolutions to the number of Monte Carlo trials. It is noticed that the estimated ability of the proposed method is better than that of Gr-SBL and the one-bit AN method with a single snapshot but inferior to that of the one-bit MUSIC method. Nonetheless, when  $T = 10$ , the estimation performance of the proposed method is higher than that of the one-bit MUSIC.

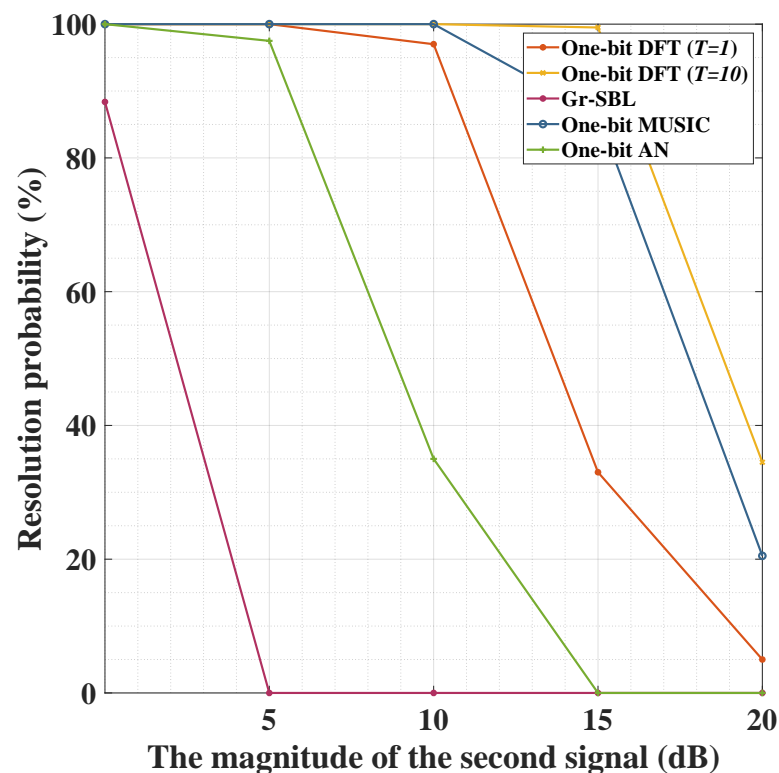


Figure 8. The variation curve of resolution with varying signal magnitude differences among all methods, where SNR = 0 dB.

## 5. Conclusions

In this paper, taking advantage of the fact that large-scale antenna arrays can greatly improve the resolution of spectrum analysis based on DFT, a novel single-snapshot one-bit DOA estimation method for MULA is proposed. The theoretical analysis and simulation verification shows that the DFT spectrum of the data received by MULA after one-bit quantization still has an obvious peak at the position containing the incident angle information. The initial DOA estimation can be derived with high precision based on the position of the peak, and the estimation precision can be enhanced with a simple phase-rotation procedure. Furthermore, the calculation stages of this method in multiple snapshot situations are analyzed. Unlike the previous one-bit DOA estimate methods, the proposed method does not require nonlinear optimization, iterative solutions, or any other complex operations, and it has the benefit of having an extremely low computing complexity. Finally, the effectiveness of the proposed method is validated with a large number of simulation experiments and an analysis of the results.

**Author Contributions:** S.G.'s contribution is conceptualization, investigation, methodology, software, and writing the original manuscript. C.F.'s contribution is conceptualization, methodology, and reviewing manuscript. J.W.'s contribution is reviewing and editing manuscript. X.H.'s contribution is conceptualization, methodology, and resources. All authors have read and agreed to the published version of the manuscript.

**Funding:** This research received no external funding.

**Institutional Review Board Statement:** Not applicable.

**Informed Consent Statement:** Not applicable.

**Data Availability Statement:** Not applicable.

**Conflicts of Interest:** The authors declare no conflict of interest.

## Abbreviations

The following abbreviations are used in this manuscript:

DOA	Direction of arrival;
MULA	Massive uniform linear arrays;
DFT	Discrete Fourier transform;
Gr-SBL	Generalized sparse Bayesian learning;
one-bit AN	One-bit quantization based on atomic norm minimization;
$ \cdot $	Modulo operator;
$\text{Re}(\cdot)$	Real part;
$\text{Im}(\cdot)$	Imaginary part;
$\mathbf{E}[\cdot]$	Expectation;
$[\mathbf{R}]_{pq}$	$pq$ -th element of matrix $\mathbf{R}$ ;
$\mathbf{R}_{(q,\cdot)}$	$q$ -th row of matrix $\mathbf{R}$ ;
$[\mathbf{x}]_q$	$q$ -th element of vector $\mathbf{x}$ ;
$\text{diag}(\cdot)$	Diagonal operator.

## References

- Luo, J.; Zhang, Y.; Yang, J.; Zhang, D.; Zhang, Y.; Zhang, Y.; Huang, Y.; Jakobsson, A. Online Sparse DOA Estimation Based on Sub-Aperture Recursive LASSO for TDM-MIMO Radar. *Remote Sens.* **2022**, *14*, 2133. [\[CrossRef\]](#)
- Wang, H.; Wang, J.; Jiang, J.; Liao, K.; Xie, N. Target Detection and DOA Estimation for Passive Bistatic Radar in the Presence of Residual Interference. *Remote Sens.* **2022**, *14*, 1044. [\[CrossRef\]](#)
- Lai, Y.; Zhou, H.; Zeng, Y.; Wen, B. Quantifying and reducing the DOA estimation error resulting from antenna pattern deviation for direction-finding HF radar. *Remote Sens.* **2017**, *9*, 1285. [\[CrossRef\]](#)
- Ma, T.; Du, J.; Shao, H. A Nyström-Based Low-Complexity Algorithm with Improved Effective Array Aperture for Coherent DOA Estimation in Monostatic MIMO Radar. *Remote Sens.* **2022**, *14*, 2646. [\[CrossRef\]](#)
- Liao, K.; Yu, Z.; Xie, N.; Jiang, J. Joint Estimation of Azimuth and Distance for Far-Field Multi Targets Based on Graph Signal Processing. *Remote Sens.* **2022**, *14*, 1110. [\[CrossRef\]](#)
- Liu, L.; Rao, Z. An Adaptive Lp Norm Minimization Algorithm for Direction of Arrival Estimation. *Remote Sens.* **2022**, *14*, 766. [\[CrossRef\]](#)
- Ge, S.; Fan, C.; Wang, J.; Huang, X. Robust adaptive beamforming based on sparse Bayesian learning and covariance matrix reconstruction. *IEEE Commun. Lett.* **2022**, *Early Access*. [\[CrossRef\]](#)
- Xiong, C.; Fan, C.; Huang, X. Time Reversal Linearly Constrained Minimum Power Algorithm for Direction of Arrival Estimation in Diffuse Multipath Environments. *Remote Sens.* **2020**, *12*, 3344. [\[CrossRef\]](#)
- Mao, Z.; Liu, S.; Qin, S.; Huang, Y. Cramér-Rao Bound of Joint DOA-Range Estimation for Coprime Frequency Diverse Arrays. *Remote Sens.* **2022**, *14*, 583. [\[CrossRef\]](#)
- Cheng, Z.; Tao, M.; Kam, P.Y. Channel path identification in mmWave systems with large-scale antenna arrays. *IEEE Trans. Commun.* **2020**, *68*, 5549–5562. [\[CrossRef\]](#)
- Li, Q.; Su, T.; Wu, K. Accurate DOA estimation for large-scale uniform circular array using a single snapshot. *IEEE Commun. Lett.* **2019**, *23*, 302–305. [\[CrossRef\]](#)
- Dai, Z.; Su, W.; Gu, H. A gain and phase autocalibration approach for large-scale planar antenna arrays. *IEEE Commun. Lett.* **2020**, *25*, 1645–1649. [\[CrossRef\]](#)
- Gong, Z.; Wu, L.; Zhang, Z.; Dang, J.; Zhu, B.; Jiang, H.; Li, G.Y. Joint TOA and DOA estimation with CFO compensation using large-scale array. *IEEE Trans. Signal Process.* **2021**, *69*, 4204–4218. [\[CrossRef\]](#)
- Zheng, W.; Zhang, X.; Wang, Y.; Zhou, M.; Wu, Q. Extended coprime array configuration generating large-scale antenna co-array in massive MIMO system. *IEEE Trans. Veh. Technol.* **2019**, *68*, 7841–7853. [\[CrossRef\]](#)
- Cao, R.; Liu, B.; Gao, F.; Zhang, X. A low-complex one-snapshot DOA estimation algorithm with massive ULA. *IEEE Commun. Lett.* **2017**, *21*, 1071–1074. [\[CrossRef\]](#)
- Li, B.; Zhang, X.; Li, J.; Ma, P. DOA Estimation of Non-Circular Source for Large Uniform Linear Array With a Single Snapshot: Extended DFT Method. *IEEE Commun. Lett.* **2021**, *25*, 3843–3847. [\[CrossRef\]](#)
- Liu, Y.; Hou, L.; Shen, Q.; Lv, C.; Na, S.; Qiu, T. Beam-space U-ESPRIT DOA Estimation Algorithm of Coherently Distributed Sources in Massive MIMO Systems. In Proceedings of the 2020 12th International Conference on Advanced Computational Intelligence (ICACI), Dali, China, 14–16 March 2020; pp. 126–132.
- Shafin, R.; Liu, L.; Zhang, J.; Wu, Y.C. DoA estimation and capacity analysis for 3-D millimeter wave massive-MIMO/FD-MIMO OFDM systems. *IEEE Trans. Wirel. Commun.* **2016**, *15*, 6963–6978. [\[CrossRef\]](#)
- Walden, R.H. Analog-to-digital converter survey and analysis. *IEEE J. Sel. Areas Commun.* **1999**, *17*, 539–550. [\[CrossRef\]](#)
- Wang, S.; Li, Y.; Wang, J. Multiuser detection in massive spatial modulation MIMO with low-resolution ADCs. *IEEE Trans. Wirel. Commun.* **2014**, *14*, 2156–2168. [\[CrossRef\]](#)

21. Mo, J.; Alkhateeb, A.; Abu-Surra, S.; Heath, R.W. Hybrid architectures with few-bit ADC receivers: Achievable rates and energy-rate tradeoffs. *IEEE Trans. Wirel. Commun.* **2017**, *16*, 2274–2287. [[CrossRef](#)]
22. Roth, K.; Nossek, J.A. Achievable rate and energy efficiency of hybrid and digital beamforming receivers with low resolution ADC. *IEEE J. Sel. Areas Commun.* **2017**, *35*, 2056–2068. [[CrossRef](#)]
23. Zhi, K.; Pan, C.; Ren, H.; Wang, K. Uplink achievable rate of intelligent reflecting surface-aided millimeter-wave communications with low-resolution ADC and phase noise. *IEEE Wirel. Commun. Lett.* **2020**, *10*, 654–658. [[CrossRef](#)]
24. Choi, J.; Sung, J.; Prasad, N.; Qi, X.F.; Evans, B.L.; Gatherer, A. Base station antenna selection for low-resolution ADC systems. *IEEE Trans. Commun.* **2019**, *68*, 1951–1965. [[CrossRef](#)]
25. Li, Y.; Tao, C.; Seco-Granados, G.; Mezghani, A.; Swindlehurst, A.L.; Liu, L. Channel estimation and performance analysis of one-bit massive MIMO systems. *IEEE Trans. Signal Process.* **2017**, *65*, 4075–4089. [[CrossRef](#)]
26. Jeon, Y.S.; Lee, N.; Hong, S.N.; Heath, R.W. One-bit sphere decoding for uplink massive MIMO systems with one-bit ADCs. *IEEE Trans. Wirel. Commun.* **2018**, *17*, 4509–4521. [[CrossRef](#)]
27. Jeon, Y.S.; Lee, N.; Poor, H.V. Robust data detection for MIMO systems with one-bit ADCs: A reinforcement learning approach. *IEEE Trans. Wirel. Commun.* **2019**, *19*, 1663–1676. [[CrossRef](#)]
28. Kong, C.; Mezghani, A.; Zhong, C.; Swindlehurst, A.L.; Zhang, Z. Multipair massive MIMO relaying systems with one-bit ADCs and DACs. *IEEE Trans. Signal Process.* **2018**, *66*, 2984–2997. [[CrossRef](#)]
29. Khalili, A.; Shirani, F.; Erkip, E.; Eldar, Y.C. MIMO Networks with One-Bit ADCs: Receiver Design and Communication Strategies. *IEEE Trans. Commun.* **2021**, *70*, 1580–1594. [[CrossRef](#)]
30. Cheng, Z.; He, Z.; Liao, B. Target detection performance of collocated MIMO radar with one-bit ADCs. *IEEE Signal Process. Lett.* **2019**, *26*, 1832–1836. [[CrossRef](#)]
31. Stöckle, C.; Munir, J.; Mezghani, A.; Nossek, J.A. 1-bit direction of arrival estimation based on compressed sensing. In Proceedings of the IEEE 16th International Workshop Signal Processing Advances in Wireless Communications, Stockholm, Sweden, 28 June–1 July 2015; pp. 246–250.
32. Meng, X.; Zhu, J. A generalized sparse Bayesian learning algorithm for 1-bit DOA estimation. *IEEE Commun. Lett.* **2018**, *22*, 1414–1417. [[CrossRef](#)]
33. Huang, X.; Liao, B. One-bit MUSIC. *IEEE Signal Process. Lett.* **2019**, *26*, 961–965. [[CrossRef](#)]
34. Wei, Z.; Wang, W.; Dong, F.; Liu, Q. Gridless one-bit direction-of-arrival estimation via atomic norm denoising. *IEEE Commun. Lett.* **2020**, *24*, 2177–2181. [[CrossRef](#)]
35. Li, Z.; Shi, J.; Wang, X.; Wen, F. Joint angle and frequency estimation using one-bit measurements. *Sensors* **2019**, *19*, 5422. [[CrossRef](#)] [[PubMed](#)]
36. Li, J.; Ma, P.; Zhang, X.; Zhao, G. Improved DFT algorithm for 2D DOA estimation based on 1D nested array motion. *IEEE Commun. Lett.* **2020**, *24*, 1953–1956. [[CrossRef](#)]
37. Huang, Z.; Wang, W.; Dong, F.; Wang, D. A one-snapshot localization algorithm for mixed far-field and near-field sources. *IEEE Commun. Lett.* **2020**, *24*, 1010–1014. [[CrossRef](#)]
38. Xie, H.; Gao, F.; Zhang, S.; Jin, S. A unified transmission strategy for TDD/FDD massive MIMO systems with spatial basis expansion model. *IEEE Trans. Veh. Technol.* **2016**, *66*, 3170–3184. [[CrossRef](#)]
39. Van Vleck, J.H.; Middleton, D. The spectrum of clipped noise. *Proc. IEEE* **1966**, *54*, 2–19. [[CrossRef](#)]
40. Jacovitti, G.; Neri, A. Estimation of the autocorrelation function of complex Gaussian stationary processes by amplitude clipped signals. *IEEE Trans. Inf. Theory.* **1994**, *40*, 239–245. [[CrossRef](#)]
41. Xiao, P.; Liao, B.; Deligiannis, N. Deepfpfc: A deep unfolded network for sparse signal recovery from 1-bit measurements with application to doa estimation. *Signal Process.* **2020**, *176*, 107699. [[CrossRef](#)]
42. Liu, Y.; Zhang, Z.; Zhou, C.; Yan, C.; Shi, Z. Robust Variational Bayesian Inference for Direction-of-Arrival Estimation with Sparse Array. *IEEE Trans. Veh. Technol.* **2022**, *Early Access*. [[CrossRef](#)]